AIAA JOURNAL
Vol. 51, No. 6, June 2013

Separation Control by External Acoustic Excitation at Low Reynolds Numbers

S. L. Yang* and G. R. Spedding†
University of Southern California, Los Angeles, California 90089-1191

DOI: 10.2514/1.J052191

At Reynolds numbers approaching those of micro air vehicles (both engineered and natural), the Eppler 387 airfoil (in common with many other smooth profiles) can have multiple lift and drag states at a single wing-incidence angle. Prestall hysteresis and abrupt switching between stable states result from sudden flow reattachment and the appearance of a large separation bubble. It is shown that control of the dynamics can be achieved using external acoustic forcing. Separation control, hysteresis elimination, and more than 70% increase in lift–drag ratio are obtained at certain excitation frequencies and sound pressure levels. The global flow around the wing is effectively modified, and large, stable vortical structures appear in the separated shear layer. Correlation between the effects of acoustic excitation and wind-tunnel resonance shows that the antiresonances in an enclosed chamber correspond to the largest improvement in wing performance. Implications for control and stabilization of small aircraft inside and out of enclosed boxes are considered.

Nomenclature

C_f	=	friction coefficient
c	=	chord, m
D_f	=	friction drag, N
f	=	frequency, Hz
f_s	=	separated shear-layer instability shedding frequency
q_∞	=	dynamic pressure, N/m^2
S	=	surface area
St	=	Strouhal number
St_a	=	angle-of-attack-based Strouhal number
St_{θ_s}	=	separation Strouhal number
Re	=	chord-based Reynolds number
U	=	freestream velocity, m/s
U_e	=	edge velocity of boundary layer, m/s
U_a	=	advection speed, m/s
u, v, w	=	velocity components in x, y, z directions
x, y, z	=	streamwise, spanwise, normal directions
α	=	angle of attack, deg
α_0	=	hysteresis loop, preceding angle of attack, deg
ω_y	=	spanwise vorticity, rad/s
θ_s	=	momentum thickness in separated region, m

I. Introduction

A GROWING number of micro aerial vehicles have been in development, production, and use for multiple applications. The flight regime in which many of these miniature aircraft systems operate is where the chord-based Reynolds number Re lies between 10^4 and 10^5, which is considered to be a low Re regime in aeronautics. Here, complex flow characteristics can either favorably or adversely affect wing performance. Two main approaches can be taken in this design space: either avoid it altogether, or manipulate and force the flow toward favorable conditions that maximize wing performance. In this study, the latter approach is taken, using active separation control through acoustic excitation.

Received 17 July 2012; revision received 7 December 2012; accepted for publication 4 January 2013; published online 11 April 2013.

*Graduate Student, Department of Aerospace and Mechanical Engineering; shanling.yang@usc.edu. Member AIAA.

†Professor, Department of Aerospace and Mechanical Engineering; geoff@usc.edu. Member AIAA.

At low Re, adverse pressure gradients are most likely to occur when the boundary layer is still laminar, making the flow over an airfoil susceptible to separation. When the flow has sufficient energy to overcome the combined effects of adverse pressure gradient, viscous dissipation, and change in momentum, the flow remains attached. Conversely, when the flow has insufficient energy, the flow separates from the wing surface then often transitions from a laminar to turbulent state and may then reattach as a turbulent boundary layer. In such a case, the separated region forward of the reattachment point will be termed a laminar separation bubble.

The performance of the Eppler 387, a high-performance sail plane airfoil usually used at $Re > 200,000$, has been shown to be strongly affected by the presence of a laminar separation bubble at lower Re [1]. In the regime $30,000 \leq Re \leq 80,000$, the E387 has complex flow characteristics where the lift–drag curves show prestall hysteresis and abrupt jumps between what appear to be multiple performance envelopes due to flow separation and reattachment, as seen in Fig. 1. Numerous laminar airfoils also experience such behavior in similar Re regimes [2,3]. These airfoils can have more than one lift or drag state at a single angle of attack. In Fig. 1, there appear to be two sets of curves to which the $C_L(C_D)$ polar may be attracted. Small perturbations can lead to a transition from one to another of what we shall term bistable state. Previous work [4] has shown that state switching corresponds to the presence or absence of reattachment and that the process is close to two-dimensional or spanwise uniform [5].

Because flow separation and reattachment both strongly affect wing performance, separation control is of clear practical significance. Active separation control involves introducing an external energy source to supplement that of the boundary layer, and common methods include external and internal acoustic excitation and vibrating wires as well as flaps, blowing, bleeding, and synthetic jets. The basis for efficient energy-based mechanisms to induce separation control is boundary-layer receptivity, when a particular disturbance such as an acoustic pressure wave or vortex structure can interact with the boundary layer and establish its signature in the resulting disturbed flow. When the initial disturbances are sufficiently large, they can grow nonlinearly and result in turbulent flow. When they are small, they can still excite disturbances in the boundary layer, such as Tollmien–Schlichting waves [6].

When the boundary layer does separate, the detached shear-layer is susceptible to Kelvin–Helmholtz (K–H) mode instabilities. The unstable waves grow, and their roll-up into coherent structures and transition to turbulence are associated with a high degree of unsteadiness and facilitation of the reattachment process as high-momentum fluid from the external flow is swept into the region close to the airfoil surface [7]. Because the possible flow reattachment is

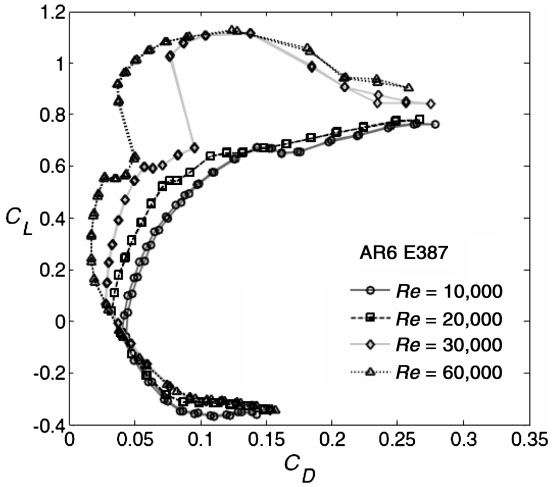

Fig. 1 Bistable states in C_L-C_D polars for the E387 wing [4].

critical to the selection of bistable state alternatives, proposed flow-control strategies should be targeted at both wall-bounded and free shear-layer modes.

Several studies have focused on external acoustic excitation as a means to modify the flow and control separation around a wing at various Re and in various flow states. External forcing at single-frequency tones has been shown to effectively change wing performance in the range of $25,000 \leq Re \leq 800,000$ by increasing lift at particular angles of attack [2,8–10], tripping the flow from low- to high-lift states [2], diminishing the size of the hysteresis loop in lift–drag curves [2], reducing the tendency toward flow separation [8,9], and changing the basic behavior of the laminar separation bubble and turbulent boundary layer [11]. The effects of external acoustic excitation have been shown in [2,8] to be strongly correlated with wind-tunnel test-section resonances.

Previous literature results on acoustic excitation at low and moderate Re and prestall and poststall α show the dependence of optimum excitation frequencies on Re, α, and the dominant intrinsic instabilities in the flow. The optimum excitation frequency has been found to increase with increasing Re or increasing α [11], while the range of effective excitation frequencies has been found to increase with increasing Re or decreasing α [11,12]. It has also been suggested that the optimum excitation frequencies correspond to the most-amplified instabilities in the separated region. For prestall and immediately poststall α, K–H instabilities dominate the separated shear region, and so the optimum excitation frequencies have been reported to correspond to these shear-layer instability frequencies [10,12–15]. For large poststall α, the dominating instabilities are due to free-wake vortices, when the optimum frequencies correspond to the vortex shedding frequencies [12,16].

The excitation frequencies can be expressed as a Strouhal number:

$$St = \frac{fc}{U} \tag{1}$$

where f is the shedding or excitation frequency, c is the chord length, and U is the freestream velocity. Laminar separation was observed to be most effectively reduced when the parameter $St/Re^{1/2}$ was between 0.02 and 0.03, based on the excitation frequency [11,13]. Recalling that the laminar boundary-layer thickness over a flat plate, $\delta \propto Re^{1/2}$, then a $St/Re^{1/2}$ scaling implies that an important length scale is set by the boundary-layer thickness δ.

St from Eq. (1) uses the chord length as the length scale and is associated with shedding on convective time and length scales. If the predominant scaling is instead determined by the size of the wake behind the body (perhaps more suitable for airfoils at high α [17]), then the projected height of the airfoil is used as the length scale, and so an alternative Strouhal number is

$$St_\alpha = \frac{fc \sin \alpha}{U} \tag{2}$$

Finally, if the laminar separation bubble itself sets conditions for subsequent growth of disturbances, then we may define

$$St_{\theta_s} = \frac{f\theta_s}{U_e} \tag{3}$$

where θ_s is the momentum thickness of the separated region, and U_e is the edge velocity of the boundary layer at the bubble edge [18]. An optimum range of St_{θ_s} has been reported to be between 0.008 and 0.016 [18].

This paper provides a study on the effects of external acoustic excitation on the forces and flowfields of an E387 wing in an Re regime where prestall hysteresis and abrupt switching of bistable states occur. At low Re, the aerodynamic performance (C_L, C_D) of the E387 and many other smooth airfoils is notoriously sensitive to small changes in environmental and/or boundary conditions, and this study reports the first of a series of experiments to unambiguously establish the basic flow conditions associated with the force variation, with a view to exploiting this sensitivity for control. If successful, then internal acoustic forcing can be examined for the same wing, and significant variations in lift and drag could, in principle, be generated with no moving parts on the wing.

II. Materials and Methods

A. Experimental Setup

Experiments were performed in a closed-loop wind tunnel with an octagonal test section of wall-to-wall width 1.37 m, length 5.7 m, and area contraction ratio of 7 to 1. The empty test-section turbulence level is 0.025% for spectral frequencies between $2 \leq f \leq 200$ Hz in the freestream velocity range $5 \leq U \leq 26$ m/s. U at any point in a given cross section deviates by no more than 0.5% from the mean for that cross section [19]. The wing was computer numerical control-machined from a solid aluminum block with $AR = 5.8$ (span $b = 52.7$ cm and chord $c = 9$ cm) with an Eppler 387 airfoil section. The (x, y, z) coordinate system is as follows: x is the streamwise direction, y is the spanwise direction, and z is the normal direction, with the origin at the leading edge and midspan (Fig. 2).

External acoustic forcing was accomplished using a SolidDrive SD1sm speaker, which was attached to the outside of the wind-tunnel test section upstream of the wing model. The SD1sm has a usable frequency response range of 60 Hz to 15 kHz and uses neodymium magnets and dual symmetrically opposed motors to convert audio signals into vibrations, which are transferred into solid surfaces upon direct contact. Placing the speaker on the outer wall of the

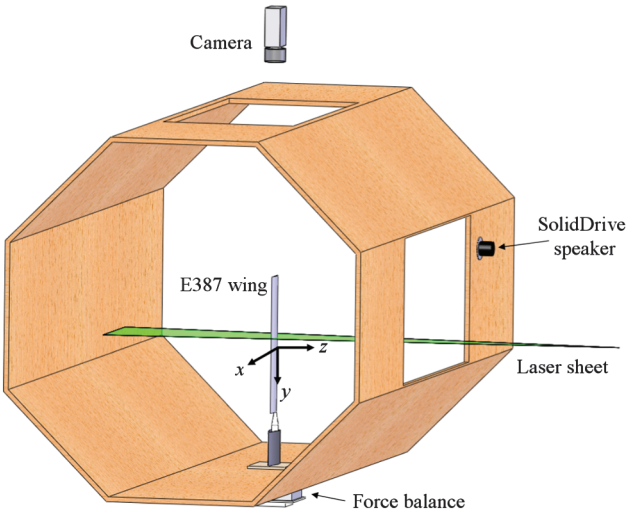

Fig. 2 Wind-tunnel setup; (x,y,z) are streamwise, spanwise, and normal directions; origin is at leading edge and midspan.

wind-tunnel test section converts the entire test section into an acoustic chamber. The vibrations from the speaker did not impact the structure of the wind tunnel. Sine waves from a waveform generator were amplified by an adjustable-gain Pyle Pro PCA1 2×15 W stereo power amplifier with a frequency response of 20 Hz to 40 kHz ± 3 dB and 0.3% total harmonic distortion. The frequency and peak-to-peak voltage amplitude of the sine wave were changed directly from the waveform generator.

A 4944 B&K pressure-field microphone, which has a pressure-field response of ± 2 dB between 16 Hz $\leq f \leq$ 70 kHz, was used to obtain acoustic measurements for the wind-tunnel resonance study. A 4954-B B&K free-field microphone, which has a free-field response of ± 3 dB between 9 Hz $\leq f \leq$ 100 kHz, was used to obtain all other acoustic measurements. Both microphones were calibrated using a B&K 4231 Acoustic Calibrator.

B. Force Balance

Lift and drag forces were measured with a custom cruciform-shaped force balance described in [19,20], placed below the wind-tunnel floor. The force balance was capable of measuring lift, drag, and pitching moment. Measurements were averaged over 8000 samples at a sampling rate of 1000 Hz. Careful calibration procedures were performed each day before data acquisition, and static calibrations were performed from 0 to 360 mN in 4 mN steps at different moment arms. The electromechanical force-balance measurement has an expected uncertainty of 0.1 mN. The friction coefficient for a Blasius boundary layer on a flat plate is

$$C_f = \frac{1.328}{\sqrt{Re_x}} \tag{4}$$

and the drag is

$$D_f = C_f q_\infty S \tag{5}$$

where q_∞ is the dynamic pressure. For a flat plate, the same size as the E387 wing at 0 deg of incidence would be 11 mN. In force-balance measurements, α was varied from -10 to 20 deg then back down to -10 deg in steps of 1 deg outside of the hysteresis loop region and in steps of 0.1 deg in the hysteresis loop region, and for each Re at least three tests were performed and results were averaged.

C. Particle Imaging Velocimetry

Particle image velocimetry (PIV) was used to estimate velocity components (u, w) in the two-dimensional plane (x, z) (Fig. 2). A Continuum Surelite II dual-head Nd:YAG laser was used to generate pulse pairs separated by exposure times $\delta t = 100$–300 μs. The two coaxial laser beams were converted to sheets of slowly varying thickness through a series of convergent cylindrical–cylindrical lenses. The flow was seeded with 1 μm smoke particles from a Colt 4 smoke generator and imaged onto a Kodak ES 1.0 1008×1018 dual-frame charge-coupled-device array camera.

PIV processing used a variant of the customized correlation imaging velocimetry algorithms described in [21,22]. A smoothed spline interpolated cross-correlation function was directly fit with the equivalent splined auto-correlation functions from the same data. Obviously incorrect vectors that passed by an automated rejection criterion were manually removed, and the raw displacement vector field was reinterpolated back onto a complete rectangular grid with the same smoothing spline function [23]. The spline coefficients are differentiated analytically to yield velocity gradient data. The uncertainty does not depend on velocity magnitude but is fixed in fractions of a pixel, but when rescaled to conditions reported here, we may expect uncertainties of 0.5–5% in $\{u, w\}$ and about 10% in gradient-based quantities, such as the spanwise vorticity:

$$\omega_y = \frac{\partial w}{\partial x} - \frac{\partial u}{\partial z} \tag{6}$$

which is displayed on a discrete color bar whose step size is set to the measurement uncertainty.

D. Acoustic Excitation at Constant Amplitude and Constant Sound Pressure Level

The effects of different excitation frequencies f_e on lift and drag forces at $Re = 40,000$ and 60,000 were examined. At each Re, a value of α_0 immediately preceding the hysteresis loop was chosen. For $Re = 40,000$, $\alpha_0 = 10$ deg, and for $Re = 60,000$, $\alpha_0 = 8$ deg. For the acoustic study at constant amplitude, f_e from the waveform generator was varied while keeping both the waveform generator peak-to-peak voltage amplitude and the power amplifier volume constant. Consequently, the sound pressure level (SPL) at a given location in the wind tunnel was not constant for this portion of the study.

For the acoustic study at constant SPL, the power amplifier was kept at a constant volume setting while the peak-to-peak voltage amplitude levels from the waveform generator were varied at each f_e to yield a constant SPL measured at the wing leading edge and midspan. The excitation frequencies that produced maximum improvements in aerodynamic performance are termed optimal, or easily excitable, frequencies, denoted as f_e^*. We note that they may be local optima in a multiparameter space. Frequencies that made the least improvements are considered to be uneasily excitable frequencies and are denoted as f_e^o. After f_e^* values were determined, the SPL was varied by changing the waveform generator peak-to-peak voltage. In both the constant amplitude and constant SPL studies, the force balance measured lift and drag forces, and PIV yielded flowfield characteristics.

E. Wind-Tunnel Resonance

Because acoustic amplitudes in a closed box vary greatly in space, spatial maps of the test-section response were measured. The B&K 4944 pressure field microphone was placed inside the empty wind-tunnel test section without flow and traversed in 2 cm steps in (x, y, z) to form three planes that would intersect the wing if it were in place. The planes traversed by the microphone were the y-z plane at the quarter chord $(x/c = 0.25)$, the x-z plane at the midspan $(y/c = 0.0)$, and the x-y plane at the leading edge $(z/c = 0.0)$ (Fig. 3). The power amplifier volume and waveform generator peak-to-peak voltage level were kept constant, and four excitation frequencies were used: two values of f_e^* and two values of f_e^o. SPL values were averaged over 15,000 samples at a sampling rate of 2500 Hz.

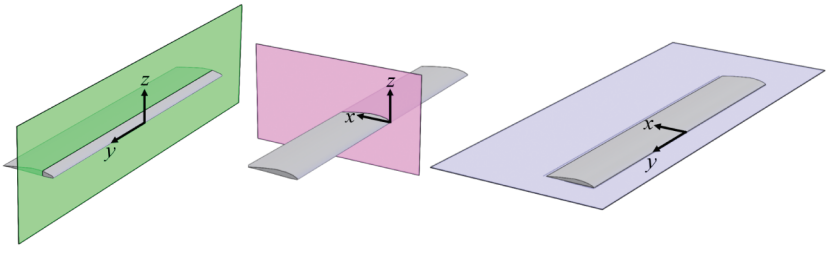

a) b) c)

Fig. 3 Wind-tunnel resonance measurement planes: a) y-z plane, b) x-z plane, c) x-y plane.

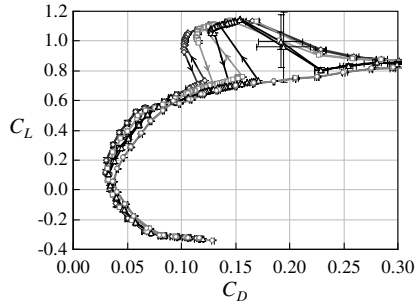

a)

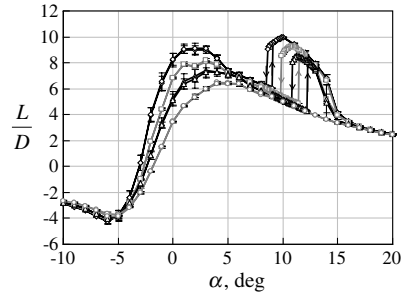

b)

Fig. 4 a) $C_L(C_D)$ curves and b) $L/D(\alpha)$ curves for the E387 at $Re =$ 30,000 (circles), 40,000 (triangles), 50,000 (squares), and 60,000 (diamonds). Error bars are the standard deviation from multiple tests.

III. Results

A. Eppler 387 Performance at Low Reynolds Numbers

Figure 4 shows the abrupt increases in lift and the decreases in drag for the E387 at particular prestall α values, which decrease as Re increases. Counterclockwise hysteresis also occurs so that the high-lift state is preserved longer as the wing incidence is decreased. Changes between separated flow and reattached flow conditions over the suction surface of the wing cause the jumps between bistable states, as observed from PIV flowfield data (not shown here). More than an 85% difference in L/D can occur over a 0.1 deg change in α (at $Re = 40,000$, the difference in L/D is 87% between 12.3 and 12.4 deg, Fig. 4b).

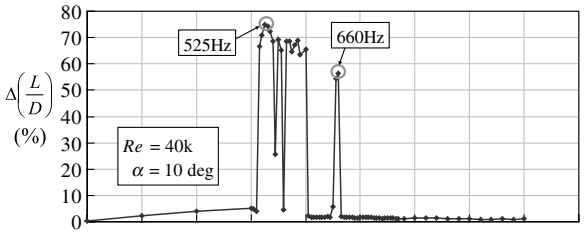

a)

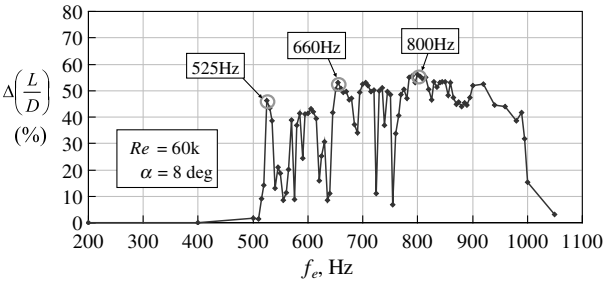

b)

Fig. 5 $\Delta(L/D)$ for different f_e at constant amplitude at $\alpha = 10$ deg at $Re =$ 40,000 (top) and at $\alpha = 8$ deg at $Re =$ 60,000 (bottom) with f_e^* values indicated.

B. Acoustic Excitation at Constant Amplitude

At both $Re = 40,000$ and 60,000, distinct increases in L/D can be observed at particular excitation frequencies, as indicated by Fig. 5, which plots the percent change in L/D with varying acoustic excitation frequencies.

Maxima in $\Delta(L/D)$ occur at $f_e^* = 525$ and 660 Hz for both $Re = 40,000$ and 60,000, but at 800 Hz there is no improvement for $Re = 40,000$. The range of f_e^* is larger for higher Re, which agrees with the observations in [11,12]. However, for the same excitation conditions, the L/D improvement is greater at $Re = 40,000$, where $\Delta(L/D)$ reaches 74% for $f_e = 525$ Hz. The maximum $\Delta(L/D)$ at $Re = 60,000$ is only 56% at $f_e = 800$ Hz. The corresponding $C_L(C_D)$ and L/D curves at the indicated f_e^* values are shown in Fig. 6.

When the flow is excited at f_e^*, hysteresis is largely eliminated for both $Re = 40,000$ and 60,000. Excitation at f_e^* removes most, but not all, of the drop in $L/D(\alpha)$ at moderate α, and the magnitude of the improvement varies with α. The higher Re case shows the closest achievement of a flat, high $\Delta(L/D)$ over a broad range of α (Fig. 6d). The original PIV images with densely seeded flow show dark lines that are the path lines of fluid originating in the relatively particle-poor boundary layer. Figure 7 compares the unforced (left column) and forced (right column) flows for $\alpha = 8$ deg at $Re = 60,000$. In Fig. 7 and subsequent plots, the $\{u, w\}$ vectors are shown with the mean flow U removed and are rescaled by an arbitrary factor for clarity. Every second vector is plotted in each direction. The unforced flow separates at a well defined location about $c/4$ from the leading edge. In the forced flow, the path line lifts slightly and late, and then marks a series of dark spots located above the airfoil surface. There is no obvious sign of a large-scale detachment. The time-average spanwise vorticity shows that, in fact, separation has occurred close to the leading edge but that the flow then reattaches to form, in the mean, a recirculation zone that is large in both x and z. The recirculation zone attaches stably to the suction surface. It can be termed a laminar separation bubble. Note that this bubble is much larger and occupies a different chordwise location from that of the well studied laminar separation bubble that appears on the SD7003 airfoil [24] and that, by contrast, has almost no dynamical significance.

C. Acoustic Excitation at Constant Sound Pressure Level

The effects of f_e on $\Delta(L/D)$ at constant SPL at $Re = 60,000$ and 40,000 together with the SPL variation with f_e in an empty wind tunnel measured at $x = 0$, $y = 0$, and $z = 0$ are shown in Fig. 8.

Figure 8c shows that the tunnel acoustic pressure is not uniform as a function of frequency, and measurements taken in the normal position of the wing show variations in SPL of up to 30 dB. These variations are due to constructive and destructive interference of primary and reflected waves in the tunnel test section, which has no special acoustic treatment of the walls. In acoustic wave fields, the gradient of pressure, $|\nabla p|$, is maximum where the pressure fluctuations cross the zero line, and this consequently is where the maximum induced particle velocity is found, 90 deg out of phase with the pressure fluctuations. When the acoustic wave field is dominated by standing waves (ultimately caused by the container geometry), nodes that correspond to zero crossings will have the lowest rms values. The high rms values, by contrast, occur where the pressure fluctuates between maximum and minimum but where the pressure gradient is close to zero. The antiresonance regions in f_e are where $\Delta(L/D)$ is highest. The flow is most easily switched to its high L/D state when the acoustic wave induced velocity field has its highest amplitude. Note that the sensitivities in Figs. 8a, 8b are adjusted for constant amplitude SPL.

The resulting performance curves from constant SPL excitation over the range of α at the three most excitable frequencies of Fig. 8b are shown in Fig. 9. Hysteresis is again eliminated, although the original dips in L/D (grey curves in Fig. 9) are not completely eliminated. Not all α experience the same magnitude of L/D improvement, similar to the results from acoustic excitation at constant amplitude. Of the three values of f_e^* (415, 520, and 675 Hz),

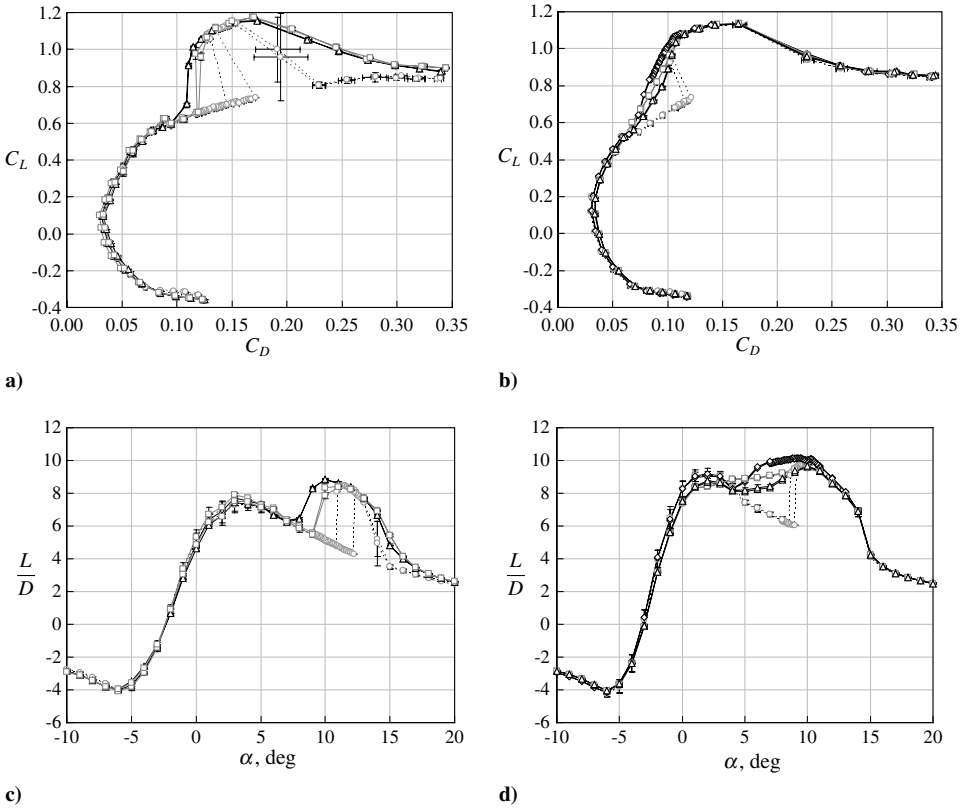

Fig. 6 $C_L(C_D)$ for a) $Re = 40{,}000$, b) $Re = 60{,}000$, and L/D for c) $Re = 40{,}000$, and d) $Re = 60{,}000$ for unexcited flow (circles), $f_e = 525$ Hz (triangles), 660 Hz (squares), and 800 Hz (diamonds).

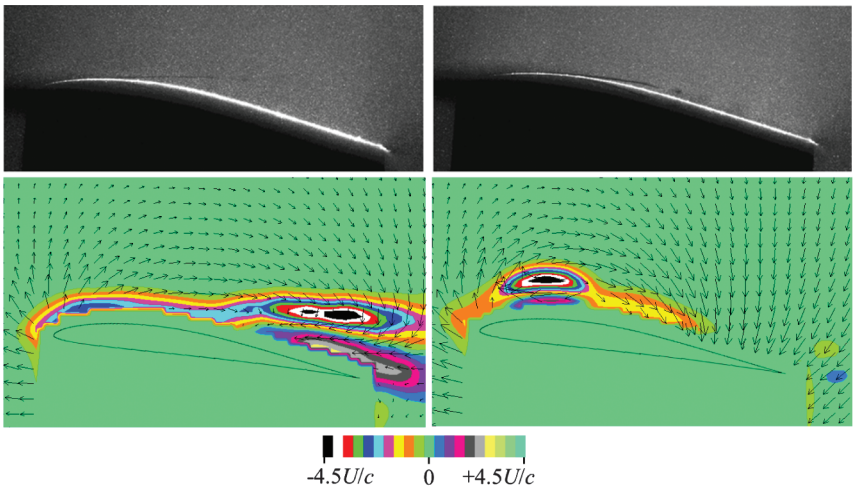

Fig. 7 Separation and spanwise vorticity for flow over E387 at $\alpha = 8$ deg and $Re = 60{,}000$ without forcing (left) and with forcing at $f_e = 800$ Hz (right).

the lower two produce better overall lift–drag curves. Qualitative results of the flowfield and corresponding spanwise vorticity field at two values of f_e^* (415 and 520 Hz) and two values of f_e^o (445 and 550 Hz) are shown in Figs. 10 and 11, respectively.

The particle images for the two f_e^o (Figs. 10b and 10d) have the same dark separation line as seen before the wing changes to the high-lift, low-drag state in normal, unexcited conditions. At the two f_e^* (Figs. 10a and 10c), the dark line, previously detached from the airfoil surface, has moved closer to the surface, and the previously noted vortical structures can be seen close to the surface starting at $x/c \approx 0.3$, most notably at 520 Hz (Fig. 10c). These vortical structures move along the suction surface of the wing from leading edge to trailing edge, as observed through a time series of acquired images. The spanwise vorticity fields (Fig. 11), obtained from the raw PIV images (Fig. 10), reveal that exciting the flow at f_e^o has no effect on the flow, which remains separated over the aft half of the airfoil, but excitation at f_e^* produces a region of circulation over the front half of the wing, corresponding to a reattached flow state.

D. Sound-Pressure-Level Dependence

The results of varying SPL on wing performance for a value of f_e^* (520 Hz) and f_e^o (550 Hz) are shown in Fig. 12. Figure 12 shows that varying the forcing amplitude at f_e^* changes the magnitude of $\Delta(L/D)$ and the range of α over which the change is seen. Changes in

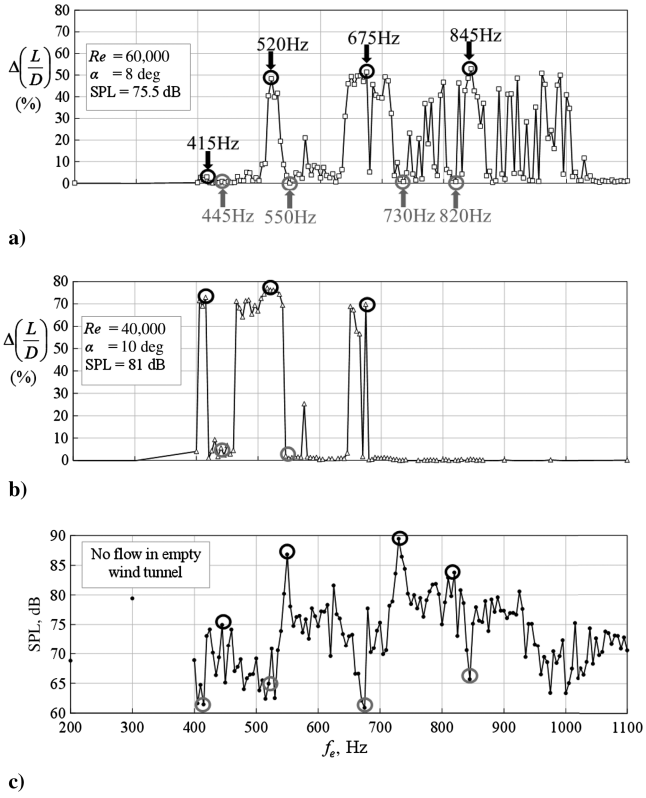

Fig. 8 Effect of f_e on $\Delta(L/D)$ at a) $Re = 60{,}000$ and b) 40,000 as well as c) corresponding wind-tunnel SPL response measured at ($x = 0$, $y = 0$, $z = 0$).

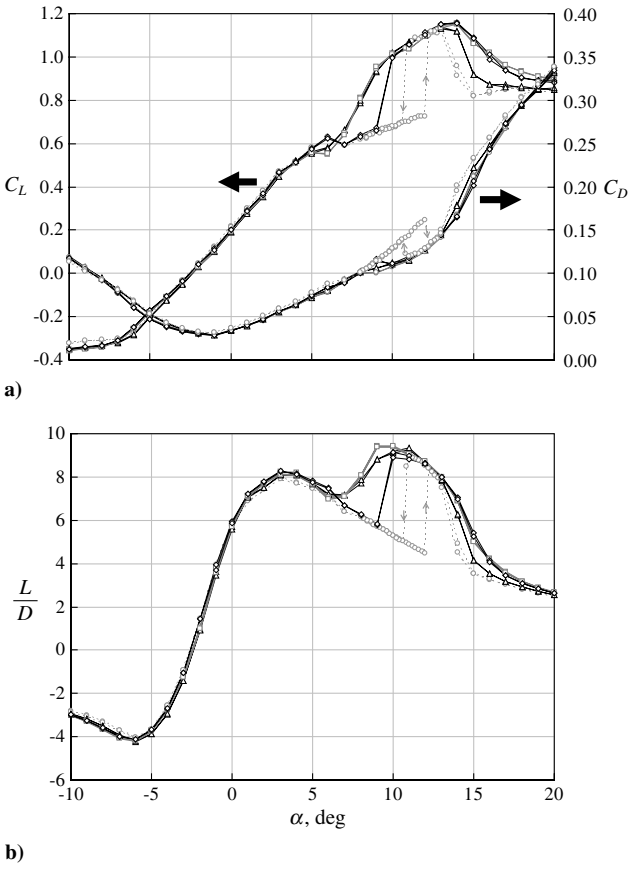

Fig. 9 Effect of f_e on a) C_L, C_D, b) L/D at $Re = 40{,}000$ for unexcited flow (circles), $f_e = 415$ Hz (triangles), 520 Hz (squares), and 675 Hz (diamonds) at constant SPL = 75.5 dB.

L/D can be obtained by forcing at f_e^o, but they require a much higher amplitude. For flow at $Re = 40,000$ and $\alpha = 10$ deg, a 77% L/D improvement is achieved with an SPL = 77.8 db at $f_e^* = 550$ Hz, but the same improvement requires a much higher SPL of 91.8 dB at $f_e^o = 550$ Hz. A 14 dB change in SPL is a 0.1 mPa change in pressure.

Varying SPL can lead to quite smooth variations in $\Delta(L/D)$, and Fig. 13 shows that SPL can be used as a control parameter for $\Delta(L/D)$ that has its own hysteresis loop, not in α (as in Figs. 4, 6, 9, and 12) but in SPL. In Fig. 13, the excitation is held constant at $f_e^* = 520$ Hz. The separated and reattached flow states are indistinguishable from those achieved with varying α.

E. Wind-Tunnel Resonance

Figures 14–16 show the spatial variation in measured SPL for constant amplitude forcing of the speaker/tunnel wall. The two f_e^* cases are shown in parts a and b and the two f_e^o cases are shown in parts c and d in each case. Figure 14 shows the SPL response in the y-z plane, Fig. 15 is the x-z plane, and Fig. 16 is the y-z plane.

The SPL varies significantly (by 15 dB) over length scales that are comparable to the span ($b \approx 6c$) in the $\{y, z\}$ plane normal to the wing and across the freestream (Fig. 14). The acoustic source is at the tunnel wall in z^+, and direct reflections will come from the opposite

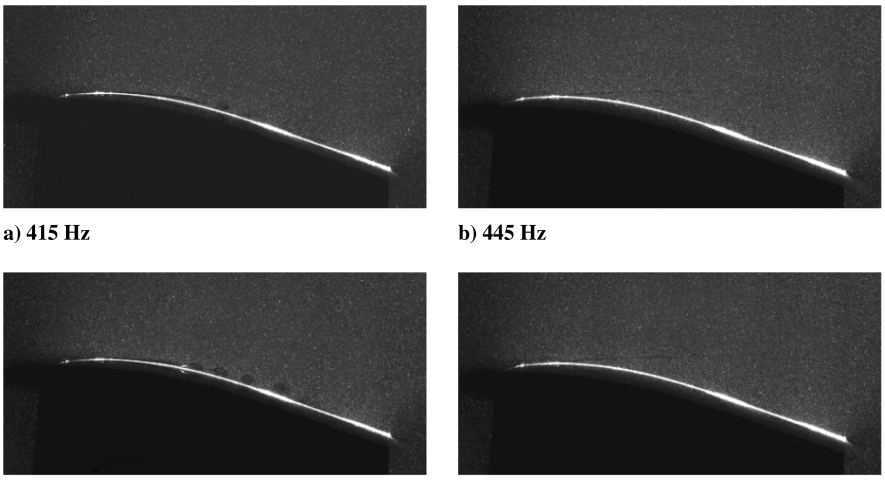

a) 415 Hz **b) 445 Hz**

c) 520 Hz **d) 550 Hz**

Fig. 10 Raw PIV images for flow at $Re = 40{,}000$ with acoustic excitation at f_e^* (Figs. 10a and 10c) and f_e^o (Figs. 10b and 10d); SPL = 75.5 dB.

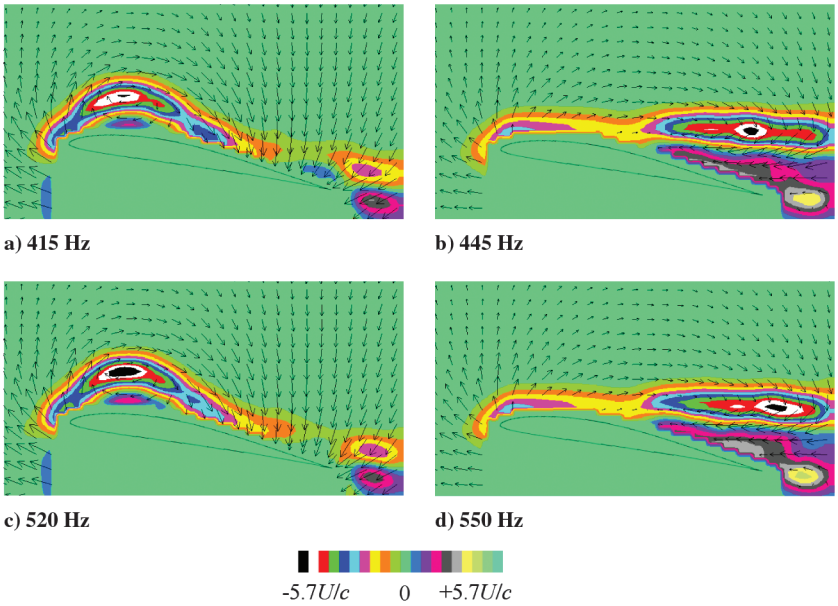

Fig. 11 Spanwise vorticity fields for flow at $Re = 40{,}000$ with acoustic excitation at f_e^* (Figs. 11a and 11c) and f_e^* (Figs. 11b and 11d); SPL = 75.5 dB.

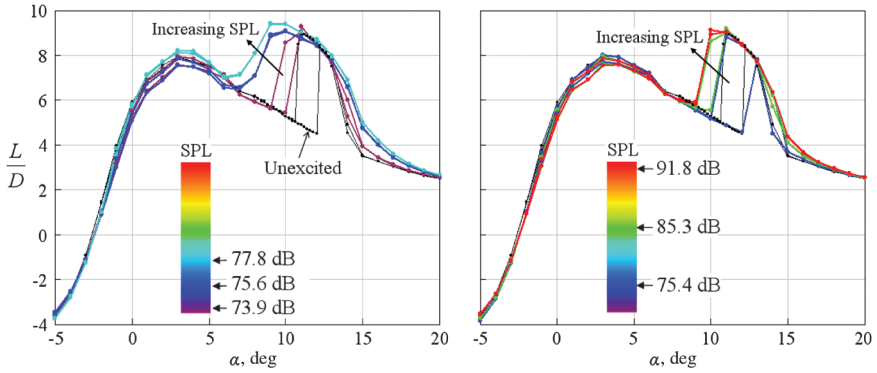

Fig. 12 $L/D(\alpha)$ for acoustic excitation at a) $f_e^* = 520$ Hz, and b) $f_e^o = 550$ Hz.

wall in z^-. The corresponding distribution in $\{x, z\}$ (Fig. 15) is more uniform, with only minor variation in x, where there are no direct reflectors. There are also smaller variations in z, which suggests that the large variations in $\{x, y\}$ of Fig. 14 come also from reflections in y. The wind-tunnel test section is octagonal, and so this is expected. In Fig. 16, the $\{x, y\}$ plane lying coplanar with the wing chord at $\alpha = 0$ deg has amplitude variations in y that are similar to those of Fig. 14 and rather small variations in x.

In reverse order, a region of SPL_{min} occurs at $y = 0$ over all x in Fig. 16 for f_e^*. In Fig. 15, this trough is at $z = 0$, uniform in x. In Fig. 14, the minimum is sharp at $z = 0, y = 0$. In this particular wing/facility geometry, spatial minima in SPL occur on the wing at midspan at this particular frequency. This SPL_{min} is associated with a maximum efficiency of flow modification. The obverse is also true; spatial maxima occur at the wing center (and flow measurement point) for the frequencies f_e^o that are least effective in disturbing the flow.

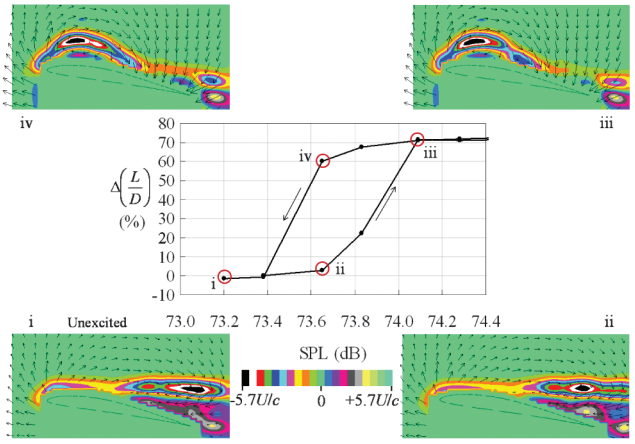

Fig. 13 Hysteresis of L/D and SPL at $Re = 40{,}000$ and $\alpha = 10$ deg. $f_e^* = 520$ Hz. Spanwise vorticity superimposed on a fluctuating velocity field is shown for the four indicated points on the hysteresis loop.

IV. Discussion

Previous literature results suggest that the values of f_e^* correspond to the most amplified instabilities in the separated shear layer (K–H instabilities) for prestall and immediately poststall α. If the values of f_e^* are used in the calculation of St in Eq. (1) and then normalized by $Re^{1/2}$, the optimum range of $St/Re^{1/2}$ for $Re = 60{,}000$ is approximately $0.015 \leq St/Re^{1/2} \leq 0.035$, and for $Re = 40{,}000$ the optimum range is $0.025 \leq St/Re^{1/2} \leq 0.045$, as shown in Fig. 17. The reported optimum range of $St/Re^{1/2}$ between 0.02 and 0.03 [11,13] coincides more with the higher Re results here. The fact that results for both Re do not overlap in $St/Re^{1/2}$ suggests that the correct scaling has not been identified.

A shear-layer frequency f_s can be obtained given a mean advection speed U_a and the spatial separation of the vortical

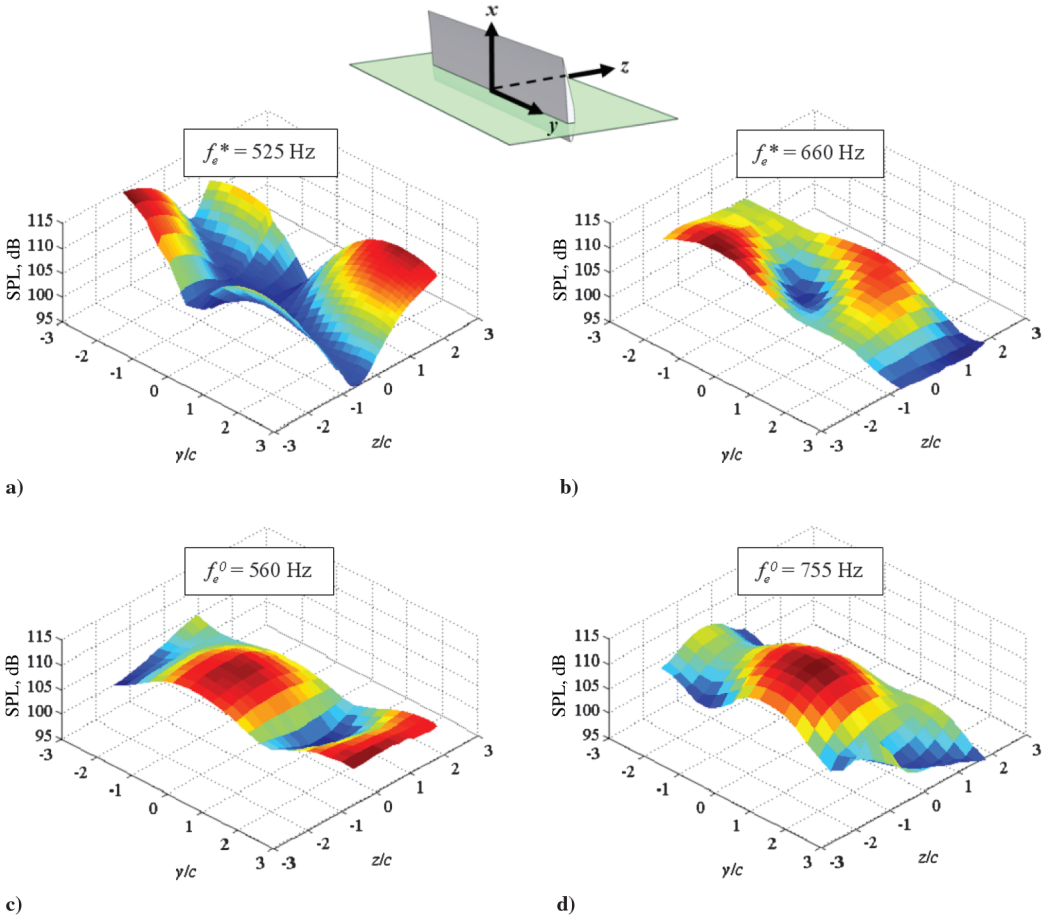

Fig. 14 Wind-tunnel resonance in the y-z plane (normal to the chord and the mean flow).

structures in the free shear layer, x_s (observable from instantaneous spanwise vorticity fields):

$$f_s = \frac{U_a}{x_s} \tag{7}$$

where x_s is the average separation between two adjacent vortical structures in the x direction, and U_a is the time-averaged streamwise velocity at the location of the vortical structures. For the case of $Re = 40,000$, using the average distance between the centers of the distinct vortices for x_s yields $f_s = 445 \pm 125$ Hz, where the uncertainty comes from using different adjacent vortices and the uncertainty in location of the vortex centers. Although this range of f_s encompasses the observed $f_e^* = 520$ Hz, the large uncertainty in f_s suggests that vortical structures in the shear layer are not shed regularly when the flow is separated. Although the vortical structures can be detected from vorticity fields, none can be clearly seen in the raw PIV images.

In contrast, when the flow is forced at f_e^*, distinct structures are evident in the raw PIV images, like Fig. 10c. If x_s is the spatial separation between the dark patches and U_a is calculated from the time-averaged velocity field at the $\{x, z\}$ location of the corresponding structures, then another shedding frequency can be calculated from Eq. (7). For the case of forcing at $f_e^* = 520$ Hz, the average f_s is equal to 1110 ± 30 Hz. This value of f_s is a second harmonic of 550 ± 30 Hz, which equals the observed $f_e^* = 520$ Hz. The uncertainty in this shedding frequency also comes only from using different adjacent vortices and the uncertainty in location of the vortex centers. The noticeably smaller uncertainty for f_s for reattached flow implies that the shedding is much steadier than that for the separated case.

The agreement of estimated f_s with the observed f_e^* suggests that forcing at intrinsic most-amplified frequencies of the free shear layer could be the most effective way to control the flow. However, if this were the case, the preferred St, or even the range of $St/Re^{1/2}$, would not vary with Re, but they do. Moreover, the proposed physical mechanism based on a resonance with f_s entirely ignores the tunnel resonance dependence.

It is most likely that the variations in effective acoustic forcing, with spatial location and with frequency, are coexisting with preferred modes in the natural (unenclosed) system. Because the full wind-tunnel/wing system is neither general nor simple, there may be limited benefit in disentangling the various contributors whose relative influence is likely measured by continuous amplitude variation, rather than having either one be completely responsible.

The quite subtle amplitude and frequency sensitivities and their dependence on the facility could explain much of the well known variation between facilities in aerodynamic performance of smooth airfoils. The test-section size and shape will determine a response map for a range of frequencies for some given acoustic source. The geometry of that response map relative to the physical wing in the tunnel will strongly affect the frequency response and sensitivity of the system. For example, when the speaker was moved $x = 3c$ upstream from its original location, some values of f_e^* were unchanged, but some were not, indicating that the effectiveness and frequency selection of external acoustic forcing depends on the geometry and corresponding nodes of standing waves in an enclosed section. When acoustic sources include not only external noise but also the wind-tunnel fan and motor assembly, it is small wonder that observations vary.

Of more practical interest will be responses that are not strong functions of reflected acoustic waves, and this could be arranged outside of a tunnel in free flight or in a specialized open-section, anechoic tunnel. Because we would like to pursue the possibility of localized forcing from sources inside the wing, it is possible that alternative experiments could succeed where reflections from low-amplitude, local forcing are not strongly influenced by reflection.

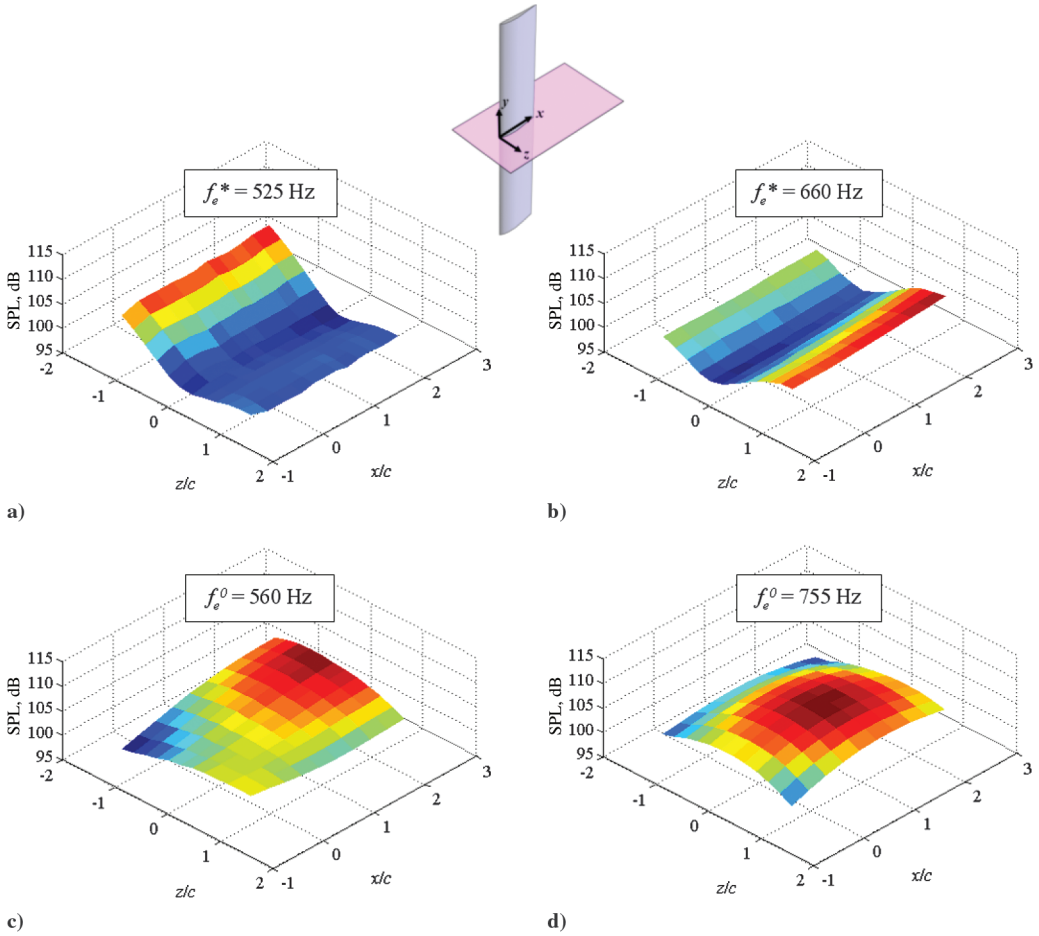

Fig. 15 Wind-tunnel resonance in the x-z plane (parallel with the chord and the freestream).

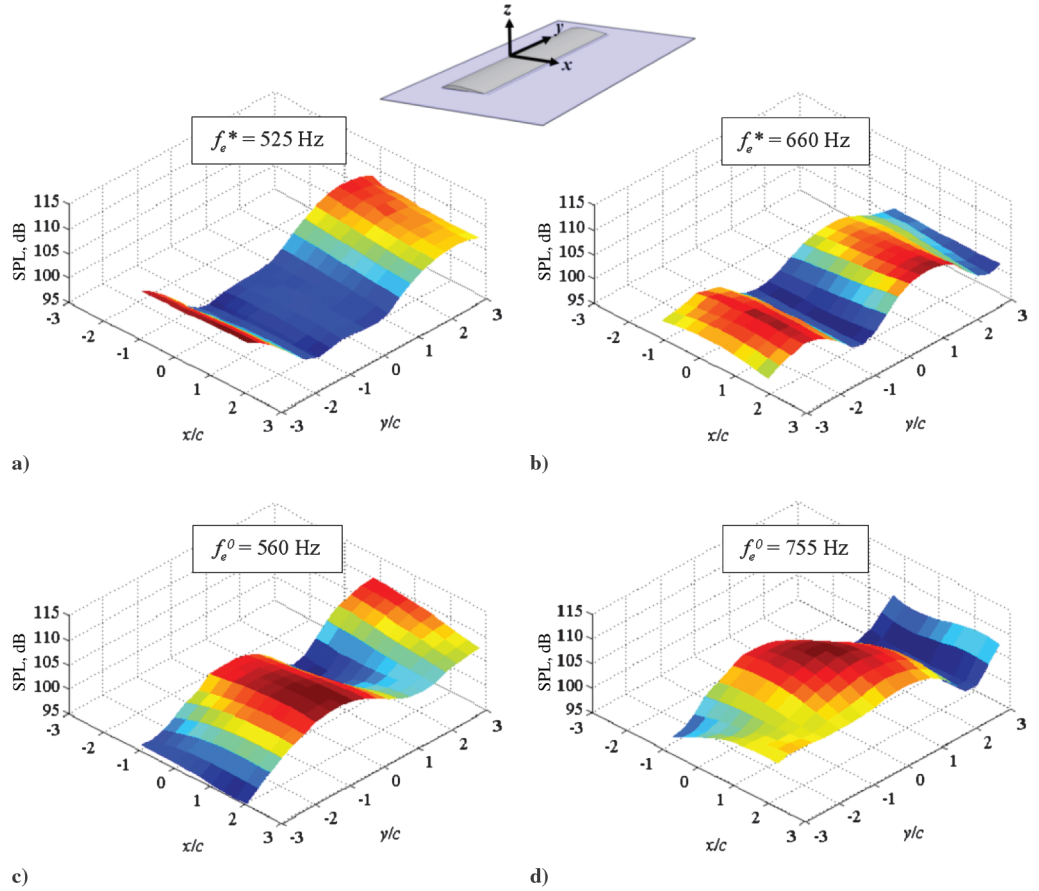

Fig. 16 Wind-tunnel resonance in the x-z plane (parallel with the chord and with the span).

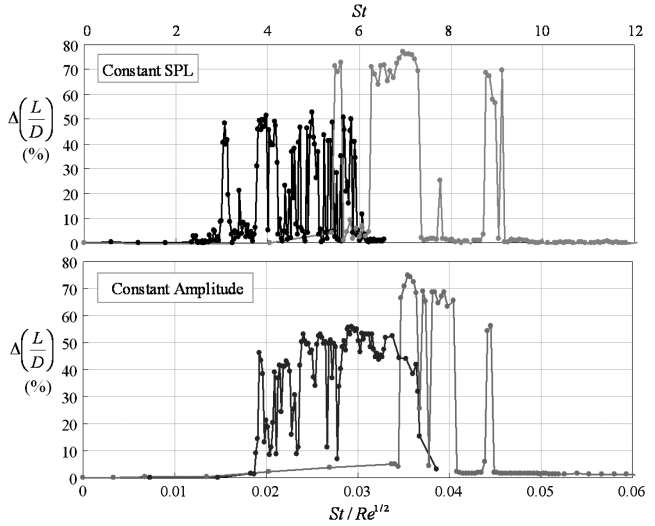

Fig. 17 $\Delta(L/D)$ as a function of St and $St/Re^{1/2}$ for $Re = 60{,}000$ (black) and $Re = 40{,}000$ (gray) for constant SPL study (top) and constant amplitude study (bottom).

V. Conclusions

The distinct jumps between bistable states and prestall hysteresis of the E387 wing, particularly in the Re regime $40,000 \leq Re \leq 60,000$, can be either provoked or eliminated by acoustic excitation at optimum excitation frequencies, yielding more than a 70% increase in L/D. Forcing at these optimum frequencies also completely changes the global flow over the wing by reattaching the formerly separated flow and forming a laminar separation bubble. Improvement by acoustic excitation is a function of f_e and sound press level, and in this experiment, optimum excitation values f_e^* correlate with wind-tunnel antiresonances. Although f_e^* and associated St^* are not inconsistent with previous literature results, the correct Re scaling is not apparent. The documented dependence on test-section geometry and acoustic resonance could explain many of the previous discrepancies in the literature at similar Re, corroborating and extending the previous observations also found in the literature. Further experiments using local on-wing forcing may help to distinguish the different effects in an open flow.

Acknowledgments

This research was supported through a National Science Foundation fellowship and the U.S. Air Force Office of Scientific Research grant FA 9550-11-1-0106, together with internal University of Southern California grants for undergraduate research and the Rose Hills Foundation.

References

[1] McGhee, R. J., Walker, B. S., and Millard, B. F., "Experimental Results for the Eppler 387 Airfoil at Low Reynolds Numbers in the Langley Low-Turbulence Pressure Tunnel," NASA TM-4062, 1988, pp. 25–26.

[2] Grundy, T. M., Keefe, G. P., and Lowson, M. V., "Effects of Acoustic Disturbances on Low *Re* Aerofoil Flows," *Fixed and Flapping Wing Aerodynamics for Micro Air Vehicle Applications*, Vol. 195, Progress in Astronautics and Aeronautics, AIAA, Reston, VA, 2001, pp. 91–112.

[3] Simons, M., *Model Aircraft Aerodynamics*, 4th ed., Special Interest Model Books, Dorset, England, U.K., 1999, pp. 227–259.

[4] Spedding, G. R., and McArthur, J., "Span Efficiencies of Wings at Low Reynolds Number," *Journal of Aircraft*, Vol. 47, No. 1, 2011, pp. 120–128. doi:10.2514/1.44247

[5] Yang, S. L., and Spedding, G. R., "Spanwise Variation in Wing Circulation and Drag Measurement of Wings at Moderate Reynolds Number," *Journal of Aircraft* (in press).

[6] Reshotko, E., "Boundary-Layer Stability and Transition," *Annual Review of Fluid Mechanics*, Vol. 8, 1976, pp. 311–349. doi:10.1146/annurev.fl.08.010176.001523

[7] Lin, J. C. M., and Pauley, L. L., "Low-Reynolds Number Separation on an Airfoil," *AIAA Journal*, Vol. 34, No. 8, 1996, pp. 1570–1577. doi:10.2514/3.13273

[8] Zaman, K. B. M. Q., and Bar-Sever, A., "Effect of Acoustic Excitation on the Flow Over a Low-*Re* Airfoil," *Journal of Fluid Mechanics*, Vol. 182, 1987, pp. 127–148. doi:10.1017/S0022112087002271

[9] Ahuja, K. K., Whipkey, R. R., and Jones, G. S., "Control of Turbulent Boundary Layer Flows by Sound," *AIAA 8th Aeroacoustics Conference*, AIAA Paper 1983-0726, April 1983.

[10] Ahuja, K. K., and Burrin, R. H., "Control of Flow Separation by Sound," *AIAA/NASA 9th Aeroacoustics Conference*, AIAA Paper 1984-2298, Oct. 1984.

[11] Zaman, K. B. M. Q., and McKinzie, D. J., "Control of Laminar Separation over Airfoils by Acoustic Excitation," *27th Aerospace Sciences Meeting*, AIAA Paper 1989-0565, Jan. 1989.

[12] Hsiao, F. B., Jih, J. J., and Shyu, R. N., "The Effect of Acoustics on Flow Passing a High-AOA Airfoil," *Journal of Sound and Vibration*, Vol. 199, No. 2, 1997, pp. 177–188. doi:10.1006/jsvi.1996.0618

[13] Yarusevych, S., Kawall, J. G., and Sullivan, P. E., "Influence of Acoustic Excitation on Airfoil Performance at Low Reynolds Numbers," *Proceedings of the 23rd International Council of the Aeronautical Sciences Congress*, Toronto, International Council of the Aeronautical Sciences, Germany, Sept. 2002, pp. 1–10.

[14] Zaman, K. B. M. Q., "Effect of Acoustic Excitation on Stalled Flows over an Airfoil," *AIAA 13th Aeroacoustics Conference*, AIAA Paper 1990-4009, Oct. 1990.

[15] Nishioka, M., Asai, M., and Yoshida, S., "Control of Flow Separation by Acoustic Excitation," *AIAA Journal*, Vol. 28, No. 11, 1990, pp. 1909–1915. doi:10.2514/3.10498

[16] Huang, L. S., Maestrello, L., and Bryant, T. D., "Separation Control over an Airfoil at High Angles of Attack by Sound Emanating from the Surface," *AIAA 19th Fluid Dynamics, Plasma Dynamics and Lasers Conference*, AIAA Paper 1987-1261, June 1987.

[17] Roshko, A., "On the Drag and Shedding Frequency of Two-Dimensional Bluff Bodies," NACA TN-3169, 1954, pp. 1–29.

[18] McAuliffe, B. R., and Yaras, M. I., "Transition Mechanisms in Separation Bubbles Under Low- and Elevated-Freestream Turbulence," *Journal of Turbomachinery*, Vol. 132, No. 1, 2010, pp. 1–10. doi:10.1115/1.2812949

[19] Zabat, M., Farascaroli, S., Browand, F., Nestlerode, M., and Baez, J., "Drag Measurements on a Platoon of Vehicles," California Partners for Advanced Transit and Highways, Inst. of Transportation Studies, University of California UCB-ITS-PRR-93-27, Berkeley, CA, 1994.

[20] McArthur, J., "Aerodynamics of Wings at Low Reynolds Numbers," Ph.D. Dissertation, Dept. of Aerospace and Mechanical Engineering, Univ. of Southern California, Los Angeles, 2007.

[21] Fincham, A. M., and Spedding, G. R., "Low Cost, High Resolution DPIV For Measurement of Turbulent Fluid Flow," *Experiments in Fluids*, Vol. 23, No. 6, 1997, pp. 449–462. doi:10.1007/s003480050135

[22] Fincham, A., and Delerce, G., "Advanced Optimization of Correlation Imaging Velocimetry Algorithms," *Experiments in Fluids*, Vol. 45, No. 29, 2000, pp. 13–22. doi:10.1007/s003480070003

[23] Spedding, G. R., and Rignot, E. J. M., "Performance Analysis and Application of Grid Interpolation Techniques for Fluid Flows," *Experiments in Fluids*, Vol. 15, No. 6, 1993, pp. 417–430. doi:10.1007/BF00191784

[24] Radespiel, R., Windte, J., and Scholz, U., "Numerical and Experimental Flow Analysis of Moving Airfoils with Laminar Separation Bubbles," *AIAA Journal*, Vol. 45, No. 6, 2007, pp. 1346–1356. doi:10.2514/1.25913

L. Cattafesta
Associate Editor